

# Multilayered Broadband Antenna for Compact Embedded Implantable Medical Devices: Design and Characterization

Aleix Garcia-Miquel<sup>1, \*</sup>, Sergio Curto<sup>2, 3</sup>, Neus Vidal<sup>1</sup>,  
Jose M. Lopez-Villegas<sup>1</sup>, Francisco M. Ramos<sup>4</sup>, and Punit Prakash<sup>2</sup>

**Abstract**—Design and characterization of a multilayered compact implantable broadband antenna for wireless biotelemetry applications is presented in this paper. The main features of this novel design are miniaturized size, structure that allows integration of electronic circuits of the implantable medical device inside the antenna, and enhanced bandwidth that mitigates possible frequency detuning caused by heterogeneity of biological tissues. Using electromagnetic simulations based on the finite-difference time-domain method, the antenna geometry was optimized to operate in the 401–406 MHz Medical Device Radio communications service band. The proposed design was simulated implanted in a muscle tissue cuboid phantom and implanted in the arm, head, and chest of a high-resolution whole-body anatomical numerical model of an adult human male. The antenna was fabricated using low-temperature co-fired ceramic technology. Measurements validated simulation results for the antenna implanted in muscle tissue cuboid phantom. The proposed compact antenna, with dimensions of 14 mm × 16 mm × 2 mm, presented a –10 dB bandwidth of 103 MHz and 92 MHz for simulations and measurements, respectively. The proposed antenna allows integration of electronic circuit up to 10 mm × 10 mm × 0.5 mm. Specific absorption rate distributions, antenna input power, radiation pattern and the transmission channel between the proposed antenna and a half-wavelength dipole were evaluated.

## 1. INTRODUCTION

Antennas are an essential element of implantable and ingestible medical devices used in a growing number of applications for monitoring physiological parameters and wirelessly communicating with other in-body or external devices [1]. Compared to other approaches, such as inductive links, implantable antennas offer advantages of reduced invasiveness, increased transmission data rate, increased communication range, and reduced sensitivity to coils' positioning [2]. Implantable antennas have been investigated in therapeutic and diagnostic applications, including but not limited to gastrointestinal (GI) endoscopy [3], artificial hip [4] and knee [5] measurements, and monitoring of intracranial pressure [6], cardiovascular pressure [7], glaucoma [8], or blood glucose [9].

Design requirements for implantable antennas include frequency of operation, size miniaturization, tuning insensitivity, bandwidth enlargement, biocompatibility, limited power absorption in body tissue, and mechanical robustness [2]. Although size reduction is a primary design objective for practical implantable antennas, other objectives must be addressed during the design phase in order to optimize antennas for specific applications. Many implantable antennas presented in the literature have been designed to operate in the 401–406 MHz Medical Device Radio (MedRadio) communications service

---

*Received 15 December 2016, Accepted 23 March 2017, Scheduled 20 April 2017*

\* Corresponding author: Aleix Garcia-Miquel (agarcia@el.ub.edu).

<sup>1</sup> Department of Engineering, University of Barcelona, C/Martí i Franquès, 1, 08028, Barcelona, Spain. <sup>2</sup> Department of Electrical and Computer Engineering, Kansas State University, 3061 Engineering Hall, Manhattan, KS 66506, USA. <sup>3</sup> Department of Radiation Oncology, Cancer Institute, Erasmus University Medical Center, Groene Hilledijk 301, 3075 EA, Rotterdam, The Netherlands.

<sup>4</sup> Francisco Albero S.A., C/Rafael Barradas, 19, 08908 L'Hospitalet de Llobregat, Barcelona, Spain.

band approved by the Federal Communications Commission (FCC) [10–16]. However, other designs in the Industrial Scientific and Medical (ISM) bands have also been reported [17–19].

In order to achieve miniaturized implantable prototypes, various antenna structures have been investigated, including one-layer planar inverted-F antennas (PIFA) [11–13, 20], multilayer PIFA [14, 21], microstrip patch [10, 12], dipole [16], loop antenna [22], and 3D-structures [15, 23]. Although some of these designs present antenna prototypes of compact volume, they do not consider the impact of integrating electronics necessary for signal conditioning of sensor data (such as amplifiers, digital converters and transceivers), for power management circuitry and for the sensor itself [2]. Consequently, the final volume of the complete implantable medical device (IMD) with the antenna and necessary electronics will be increased, as in the work presented in [6]. A recent study of energy harvesting applications investigated an IMD with on-board integration of the antenna and signal conditioning electronics [23].

Another challenge when designing implantable antennas is the observed detuning when the device is implanted at various body locations. This work builds upon our previous studies [24, 25], where we evaluated frequency shifts caused by dispersive heterogeneity of electrical properties of tissue and distinct anatomical geometries. Results showed that a bandwidth of at least 70 MHz is required for implantable antennas based on a PIFA structure operating at the MedRadio 401–406 MHz frequency band. This value was derived from analysis of detuning and impedance mismatching of antennas implanted at various locations and depths inside the human body. Moreover, anatomical variations between individuals may also result in detuning of antenna response [24, 26]. Published research focused on PIFA bandwidth increment, such as multiband structures [13, 21, 27, 28], parasitic elements [29], additional slots on the ground plane [30] or the radiator patch [14], modification of the ground plane structure [31], and geometric variations of the feed plate silhouette [32]. However, only antennas reported in [13, 14, 21, 27] were designed to be implanted into a human body. In order to ensure biocompatibility of the IMD and to reduce induced currents and power absorbed by the human body, systems were embedded inside dielectric substrates [12].

Given the previous implantable antenna design considerations, a broadband PIFA for wireless biotelemetry applications is presented in this paper. This work attempted to achieve the following: (1) a suitably miniaturized design to improve versatility and applicability of the antenna, (2) a structure capable of integrating an IMD into the internal cavity of the antenna, and (3) an operating bandwidth of at least 70 MHz to offset detuning effects caused by heterogeneity of tissues at various locations within the human body. The proposed device, which operates in the MedRadio 401–406 MHz frequency band [33], was based on multilayer low-temperature co-fired ceramic (LTCC) technology, thereby guaranteeing a biocompatible substrate for the device [34]. LTCC technology offers the integration of internal vias and cavities that allow integrated microstructures to be embedded into the antenna [35, 36], increasing viability for designing the internal circuitry.

This paper is organized as follows. Section 2 presents the proposed antenna design and methodology. Simulated and measured results are described in Section 3, including reflection coefficient ( $S_{11}$ ), specific absorption rate (SAR), transmission channel and radiation patterns. Discussion of the results and conclusion are presented in Section 4 and Section 5, respectively.

## 2. MATERIALS AND METHODS

### 2.1. Antenna Design

The proposed antenna geometry (Fig. 1(a)) comprises four stacked layers of LTCC dielectric substrate with  $\epsilon_r = 6.7$  and  $\sigma = 0.0026$  S/m and two embedded radiators. The main radiator, which is a folded square inverted-F structure that followed the perimeter of the antenna module (Fig. 1(b)), is located between the first and second layer and between the second and third layer of the LTCC substrate. The secondary radiator consisted of a meander inverted-F structure; this radiator was located between the third and fourth layer. The two radiators shared a common ground plane, but only the main radiator was fed the incoming signal at the feed point identified in Fig. 1(b) and Fig. 1(c) and generated the first resonance peak. Due to electromagnetic coupling, part of the energy was transferred to the secondary

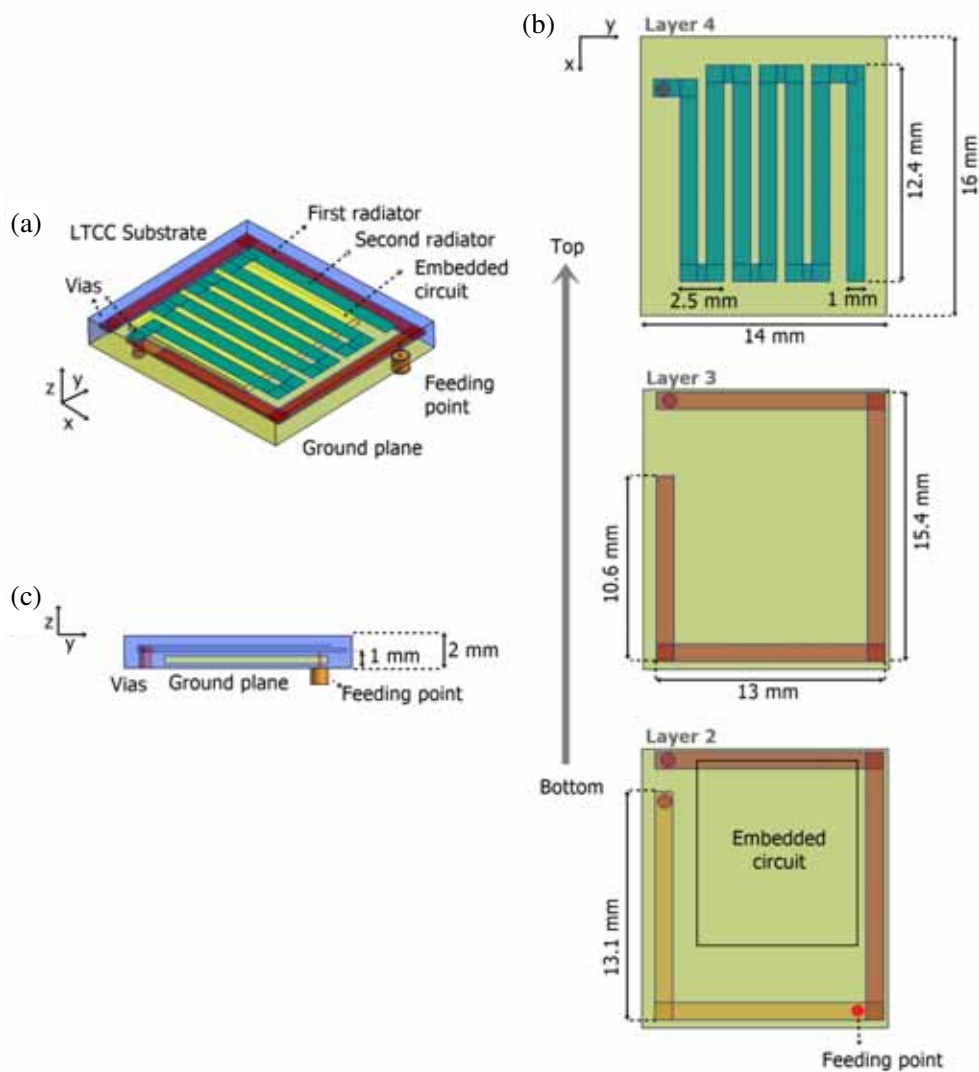


**Figure 1.** Geometry of the proposed antenna: (a) 3D view, (b) top view of each metallic layer, and (c) side view. The main radiator was located in the second and third layers, with two turns separated by 0.2 mm. The secondary radiator, a meander inverted-F structure, was located in the fourth layer. The light yellow area in (a), (b) bottom, and (c) shows an example location for embedding circuitry.

radiator, and it created a second radiation peak. The combination of the two resonance peaks resulted in bandwidth broadening. The antenna design was optimized to operate at 403 MHz when being implanted inside muscle tissue ( $\epsilon_r = 57.1$  and  $\sigma = 0.797$  S/m) [37]. The antenna has a volume of  $448 \text{ mm}^3$ , with a width of 14 mm, length of 16 mm, and thickness of 2 mm.

LTCC technology has been used for almost 20 years to produce a multilayer substrate for packing integrated circuits [35]. The fabrication method is based on processing each layer independently and then stacking and packaging them by a lamination and a firing process. This technology has shown appropriate electrical and mechanical properties and high reliability and stability, as well as allowing production of 3D-integrated microstructures [36]. LTCC technology has proven versatile for building complex multilevel channel structures, including large-volume cavities suitable for biological applications [38]. LTCC has been tested for biocompatibility and has been used in various biological applications, such as evaluation of human umbilical vein endothelial cells [33], and multi-sensor monitoring [37].

## 2.2. Methodology

Simulation results obtained in this study were based on electromagnetic modeling using the finite-difference time-domain (FDTD) method [39]. The commercially available electromagnetic simulator SEMCAD (Schmid & Partner Engineering AG) was used.

The muscle tissue cuboid phantom was modeled as a cube of 150 mm  $\times$  80 mm rectangular section and 110 mm deep. The antenna was centered with the rectangular section and implanted within the phantom at a depth of 15 mm from the edge as shown in Fig. 2(a). The antenna geometry, with the main radiator placed at the periphery, provided a wide internal space for future embedding of electronic circuits (light yellow area in Fig. 1(a), (b) [bottom], and (c)). Such electronic elements could lead to unexpected detuning due to electromagnetic coupling interaction. The electronic elements were approximated as a metallic box embedded in the prototype as a first approach to quantify their influence on the antenna performance. Metallic box volumes ranging from 0.5  $\times$  0.5  $\times$  0.5 mm<sup>3</sup> to 10  $\times$  10  $\times$  0.8 mm<sup>3</sup> and located at different positions were evaluated.

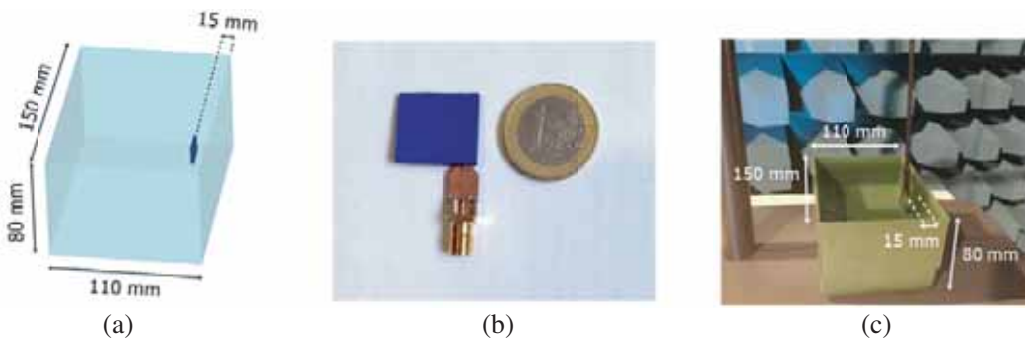


**Figure 2.** (a) Muscle tissue cuboid phantom used in simulations, (b) manufactured prototype in LTCC fed by a standard SMA connector through a coplanar wave guide launcher and (c) muscle tissue cuboid phantom used in the measurement setup.

In order to validate the design, the antenna was manufactured and measured when being implanted within a phantom at a depth of 15 mm from the edge. The phantom contained de-ionized water, salt, sugar, and hydroxyethyl cellulose as indicated in FCC guidelines for human exposure to radiofrequency electromagnetic fields [41]. Dielectric properties measurements ( $\epsilon_r = 57.2$ ,  $\sigma = 0.8$  S/m) were performed with the Agilent 85070E open-ended coaxial dielectric probe kit and the HP8720C network analyzer. In order to avoid external interferences and multipath reflections, the experimental setup was placed inside an anechoic chamber. The antenna was fed by a standard SMA connector through a coplanar wave guide launcher, as illustrated in Fig. 2(b). Experimental measurements of the reflection coefficient were also carried out with the setup shown in Fig. 2(c).

Electromagnetic simulations were employed to evaluate the proposed antenna design when being implanted at a depth of 15 mm in the arm, chest, and head of a whole-body male anatomical model to assess the detuning of antenna response caused by different body locations [24] at the same depth. The model was extracted from the Virtual Family dataset [40], which is based on high-resolution magnetic resonance images of healthy male volunteers. All tissues and organs were reconstructed as unstructured 3D-triangulated surface objects, thereby yielding high-precision images of individual body features. Antenna reflection coefficient, SAR distribution, radiation pattern and the transmission channel between the implanted antenna and an external dipole were evaluated. The quality of the transmission channel was assessed by the power received by the external dipole when being positioned at varying distances from the implanted antenna. An isotropic antenna was used to measure the received power. The effective area of the dipole was used to compare the measured electric field with the simulated received power. The far-field radiation pattern and peak gain were computed using simulations with the antenna implanted inside the homogeneous phantom block surrounded by free-space. Measurements of the radiation pattern were also carried out using the received power of the isotropic antenna in steps of 15 degrees. Normalization of both simulated and measured radiation patterns were performed for comparison purposes.

### 3. RESULTS

#### 3.1. Reflection Coefficient

Figure 3 shows the simulated and measured reflection coefficients of the antenna implanted on muscle tissue cuboid phantom at 15 mm from the edge, as shown in Fig. 2(a) and Fig. 2(c). Two resonance peaks were combined, generating a  $-10$  dB bandwidth of 103 MHz (358–461 MHz) for the simulation and 92 MHz (352–444 MHz) for the measurement.  $S_{11}$  at 403 MHz was  $-11.5$  dB and  $-16$  dB for simulation and measurement, respectively. Minor detuning to lower frequencies and bandwidth narrowing were observed in experimental results.

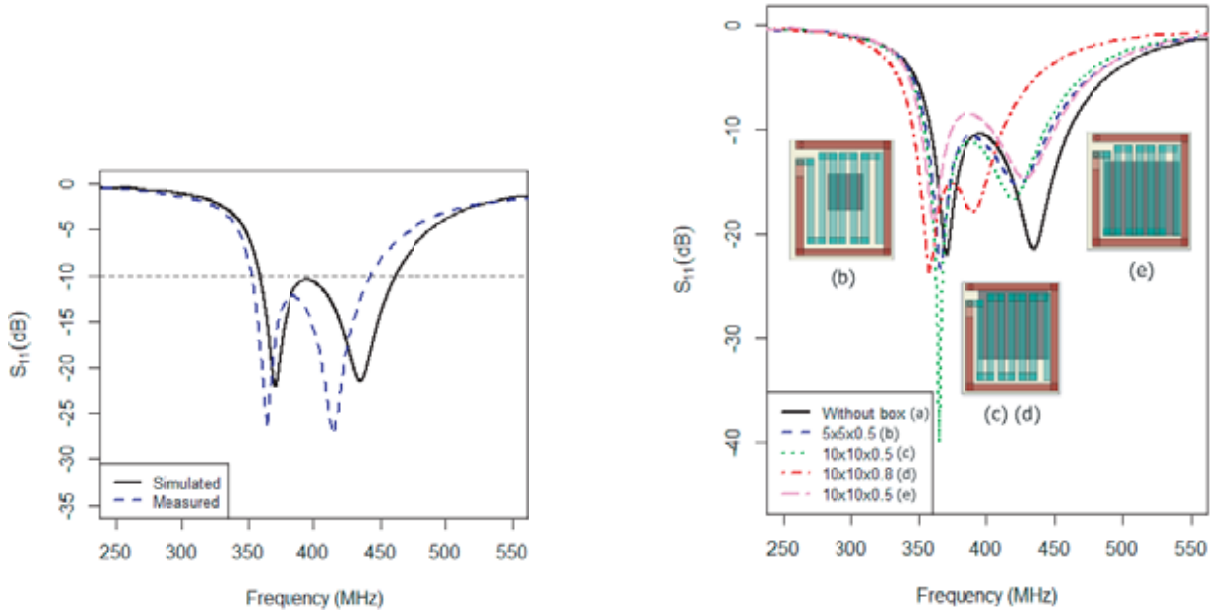


**Figure 3.**  $S_{11}$  of the (a) simulated and (b) measured antenna implanted in the muscle tissue cuboid phantom.

**Figure 4.** Simulated reflection coefficient of the antenna implanted in the muscle tissue cuboid phantom (a) without and (b)–(d) with embedded metallic boxes of varying size. The boxes' dimensions were (b)  $5 \times 5 \times 0.5$  mm, (c)  $10 \times 10 \times 0.5$  mm, (d)  $10 \times 10 \times 0.8$  mm, and (e)  $10 \times 10 \times 0.5$  mm.

Figure 4 shows the simulated antenna reflection coefficient with the antenna implanted in the muscle tissue cuboid phantom considering four different antenna locations and sizes for the internal metallic box. Differences in antenna detuning were observed with respect to the reference antenna without the internal metallic box (trace (a) in Fig. 4). For a box with dimensions  $5 \text{ mm} \times 5 \text{ mm} \times 0.5 \text{ mm}$  and located 7 mm from to the feed point (trace (b)), the  $-10$  dB bandwidth was 92 MHz (354.8–446.8 MHz). For a box with dimensions  $10 \text{ mm} \times 10 \text{ mm} \times 0.5 \text{ mm}$  and located 4.5 mm from to the feed point (trace (c)), the  $-10$  dB bandwidth was 87 MHz (354.9–442.8 MHz). When the thickness of the box increased from 0.5 mm to 0.8 mm (i.e., the embedded box was at 0.2 mm from the main radiator), a strong narrowing in the bandwidth was observed. For a box with dimensions  $10 \times 10 \times 0.8$  mm (trace (d)), the  $-10$  dB bandwidth was 67 MHz (345–412 MHz). Proximity of the metallic box to the feed point increased impedance mismatching. For a box with dimensions  $10 \text{ mm} \times 10 \text{ mm} \times 0.5 \text{ mm}$  and located 1 mm from to the feed point (trace (e)), a mismatch of  $S_{11} > -10$  dB was observed between 373.7 and 403.6 MHz, generating a  $-10$  dB bandwidth of 22.3 MHz (351.4–373.7 MHz) and 46.2 MHz (403.6–449.8 MHz).

Simulated reflection coefficients of the antenna, without embedded metallic boxes, when being implanted in the muscle tissue cuboid phantom and in the arm, chest, and head of the whole-body model are shown in Fig. 5. A shift of the resonance peak at 370 MHz of the antenna implanted into the muscle tissue cuboid phantom towards higher frequencies was observed for the antenna implanted into

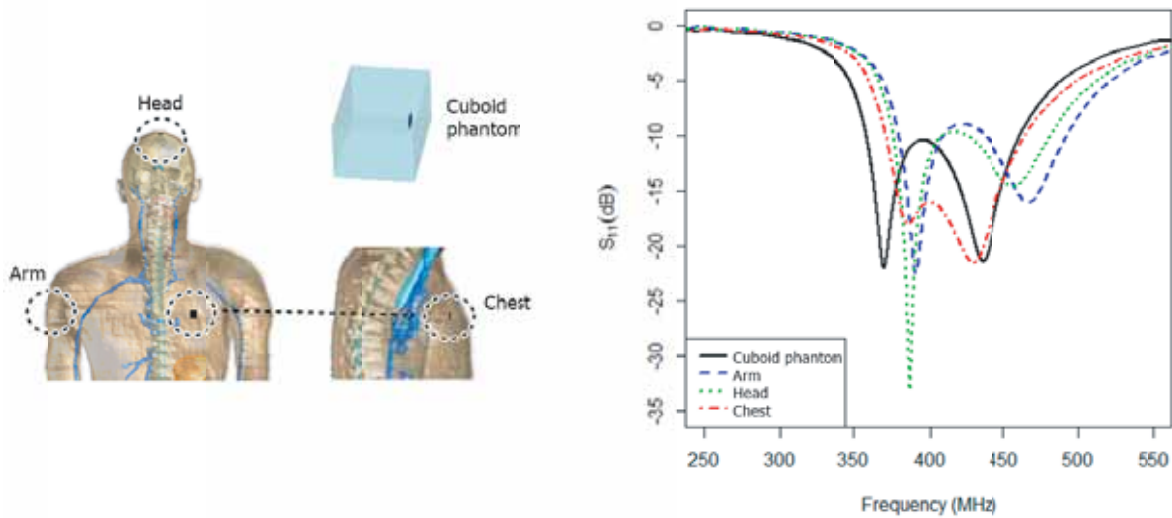


**Figure 5.** Simulated reflection coefficient of the antenna implanted inside the muscle tissue cuboid phantom and into the arm, chest and head of the anatomical male body model [37].

the anatomical body. The second resonance peak at 435 MHz for the antenna implanted into the muscle tissue cuboid phantom shifted to higher frequency when the antenna was implanted in the arm and chest and did not change significantly for the antenna implanted in the head. A combination of the two resonance peaks produced a  $-10$  dB bandwidth of 93 MHz (371.1–464.5 MHz) with a  $S_{11}$  of  $-16.1$  dB at 403 MHz for the antenna implanted into the head, while the  $-10$  dB bandwidth showed two sections 379.5–408.6 MHz and 436.7–492.3 MHz for the antenna implanted into the arm, and 375.9–407.8 MHz and 424.6–481.39 MHz for the antenna implanted into the chest.

### 3.2. Specific Absorption Rate

The 3D near-field distributions were calculated, and numerical analysis of the SAR was performed at 403 MHz. The antenna, which was numerically analyzed without an embedded metallic box, was tested in a muscle tissue cuboid phantom and in the head, chest and arm of the male anatomical model as shown in Fig. 5. For comparison with previous studies, antenna input power was set to 1 W. The 1-g and 10-g averaged peak SAR results are shown in Table 1.

In order to meet basic SAR restrictions for general public exposure (i.e., IEEE C95.1-1999 [1-g averaged SAR  $< 1.6$  W/kg] [40] and IEEE C95.1-2005 [10-g averaged SAR  $< 2$  W/kg] [41]), power delivered by the antenna had to be modified. If the highest SAR value obtained in the analysis (Table 1, in the arm) was considered, the delivered power had to decrease to 3.7 mW in order to satisfy the most restrictive SAR regulation (i.e., SAR  $< 1.6$  W/kg).

**Table 1.** Specific absorption rate (SAR) results.

Antenna location	1-g averaged		10-g averaged	
	SAR (W/kg) 1 W input power	Max. power (mW) to meet 1-g averaged SAR restriction	SAR (W/kg) 1 W input power	Max. power (mW) to meet 10-g averaged SAR restriction
Muscle tissue cuboid phantom	380.9	4.2	90.0	22.2
Arm	435.9	3.7	93.9	21.3
Chest	398.3	4.0	91.5	21.8
Head	323.6	4.9	89.0	22.5

Maximum power calculations based on SAR basic restrictions for general public exposure: IEEE C95.1-1999 (1-g averaged SAR < 1.6 W/kg) and IEEE C95.1-2005 (10-g averaged SAR < 2 W/kg). The setup and locations are presented in Section 4 (Fig. 5).

### 3.3. Transmission Channel

The transmission channel between the proposed antenna and a half-wavelength dipole was evaluated in terms of received power. The proposed antenna was located at 15 mm from the edge of the muscle tissue cuboid phantom and into various locations within the anatomical model. The same study cases as in Fig. 5 were considered. The simulated half-wavelength dipole antenna was positioned at distances ranging from 1 cm to 100 cm from the phantom-air and skin-air interfaces. In the experimental measurements, the isotropic antenna was positioned at distances ranging from 10 cm to 100 cm from the phantom-air interface as shown in Fig. 6. On the basis of SAR results and limitations (Table 1), the transmitting antenna was assumed to have an input power of 3.7 mW (i.e., the most restrictive case). Power received at the external half-wavelength dipole was obtained by the transmission coefficient, determined by the relation between available power at the transmitter implanted antenna and received power at the 50  $\Omega$  load that terminated the receiver antenna [42].



**Figure 6.** Experimental setup to measure the received electric field by the external isotropic antenna.

Results from the muscle tissue cuboid phantom and the anatomical model are illustrated in Fig. 7. Received power showed a variability of  $\pm 4$  dB when the half-wavelength dipole antenna was at 20 cm from phantom-air and skin-air interfaces for the various implanted antenna locations. Maximum deviations up to  $\pm 5$  dB were observed when the half-wavelength dipole antenna was at 100 cm from phantom-air and skin-air interfaces. The largest received power was observed when the antenna was implanted into the arm; the lowest received power was found when the antenna was located in the chest.

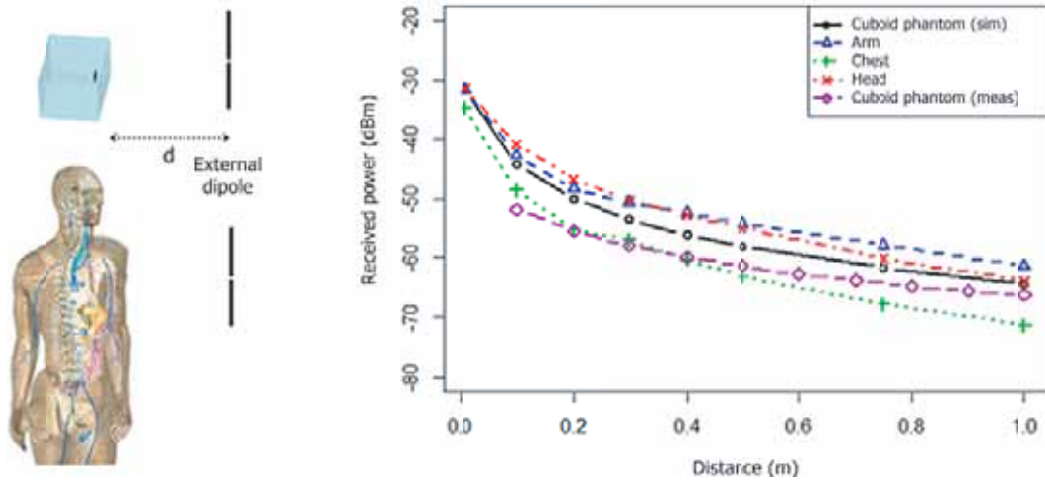
### 3.4. Radiation Pattern

Figure 8 shows the simulated and measured normalized antenna radiation patterns when being implanted in the muscle tissue cuboid phantom at 15 mm from the phantom edge for the  $xz$ -plane. The normalized received power of the isotropic external antenna in steps of 15 degrees along the  $xz$ -plane was used to perform the measured radiation pattern. The axes are detailed in Fig. 1.

Table 2 shows the main parameters for the simulated and measured radiation patterns.

**Table 2.** Main radiation pattern parameters.

<i>Parameter</i>	Simulation	Measurements
Step degree	1.66°	15°
Maximum direction	85°	45°
3 dB beamwidth	147°	120°
Front-to-back ratio	3.6 dB	1.3 dB



**Figure 7.** Power received by the external dipole as a function of distance  $d$  for the same cases as in Fig. 5. Measured results of the antenna implanted in the muscle tissue cuboid phantom are also represented.

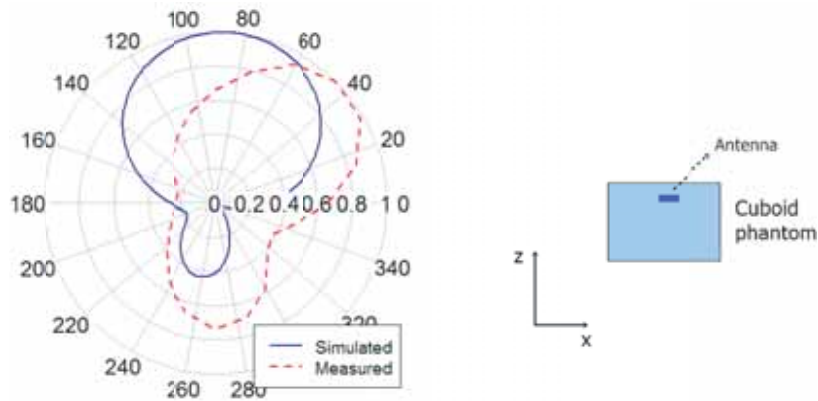


**Figure 8.** Simulated and measured normalized antenna radiation patterns (dBi) for the  $xz$ -plane with the antenna implanted in the muscle tissue cuboid phantom.

#### 4. DISCUSSION

This study was initiated to design and evaluate the feasibility of a miniaturized antenna for an IMD. The proposed design employed LTCC technology with four stacked layers and two embedded radiators. Only the main radiators were fed the incoming power signal, and energy was coupled to the second radiator. Each independent radiator generated a resonance peak. Coupling between the two radiators produced a combination of the two resonances and subsequent bandwidth enlargement. Simulated and measured models achieved a bandwidth of 103 MHz and 93 MHz, respectively. A bandwidth greater than 70 MHz was achieved in both cases, fulfilling requirements considered in previous studies [24].

The main radiator of the proposed antenna was specifically placed at the periphery of the device to allow integration of IMD electronic circuits inside the core of the antenna. The main influence of the embedded box on the antenna return loss was a slight frequency shift to lower frequencies and bandwidth narrowing. Embedded box sizes up to  $10 \times 10 \times 0.5$  mm rendered a suitable performance at the MedRadio band, with a  $-10$  dB bandwidth reduction of 15% respect the design without the box. Increasing box height to 0.8 mm produced a reduction on antenna bandwidth of 34.9%. When the box was located at a distance of 1 mm or less from the antenna feed point, unacceptable antenna mismatching was generated in the frequency of interest.

When the antenna was implanted into various locations on the human body, a shift to higher frequencies was observed for the first resonance peak. When the antenna was implanted into the arm and chest, the second resonance peak shifted to higher frequencies and the combination of the two resonances peaks was compromised. When the antenna was implanted into the head, the second resonance peak did not shift to higher frequencies and combined with the first resonance peak generating an improved matching at the frequency of interest.

SAR analysis was performed at 403 MHz for the muscle tissue cuboid phantom and implanted in the arm, in the head and in the chest of the male anatomical model. The antenna implanted in the arm generated the highest SAR for the cases of 1-g averaged SAR and 10-g averaged SAR. Based on SAR basic restrictions for general public exposure, maximum delivered power of the antenna was found to be 3.7 mW.

A half-wavelength dipole antenna was placed at various distances from the antenna implanted into the muscle tissue cuboid phantom and at various locations within the anatomical model. When the half-wavelength dipole was located at 1 cm from the phantom-air or skin-air interface, the power received at the dipole was similar for all antenna locations. For dipole to phantom-air or skin-air interface distances between 10 cm and 30 cm, the antennas implanted into the head and arm generated similar power, and the values were around 4 dB more than the antenna implanted in the tissue phantom and around 10 dB than the antenna implanted in the chest. For distances greater than 40 cm, the antenna implanted into the arm generated the highest power in the receiver half-wavelength antenna. The antenna implanted into the chest generated the lowest power in the receiver dipole for all evaluated distances. Depending on the antenna location, the surrounding tissues differed, with distinct dielectric properties and geometries, leading to unique radiation patterns for each location. The amount of lossy media surrounding the antenna and the reflections caused by tissue interfaces directly impacted the transmission channel quality. The measured results for the antenna implanted in the muscle tissue cuboid phantom show a reduction of the simulated received power around 8 dB and 1 dB at distances of 10 cm and 100 cm from the source, respectively. The conversion from an isotropic antenna to a half-wavelength dipole through the effective area is not totally accurate for regions close to the near-field, while for larger distances results converge. Another issue related to the measurements is the influence of the coaxial cable of the measurement setup in electrically small and implantable antennas, as reported in [44, 45].

A simulated peak gain of  $-32$  dB was achieved when the antenna was implanted into the muscle tissue cuboid phantom surrounded by the free-space. The radiation pattern for both simulation and measurements (Fig. 8) shows a directional performance in the positive  $z$ -axis, where the amount of lossy tissue for the microwaves to cross is lower and, therefore, the attenuation is also reduced. The measured maximum level of the normalized radiation pattern shifts  $40^\circ$  from the simulated results. A  $27^\circ$  reduction in the 3 dB beamwidth and a 2.3 dB drop in the front-to-back ratio are also observed in the measurements.

**Table 3.** Comparison of implantable antenna performances found in literature.

<i>Reported design techniques/approaches</i>	Volume (mm <sup>3</sup> )	$-10$ dB BW (MHz)	Max Gain (dB)	Designed for embedded circuit
Kim et al. [11]	10240	13	N/A	No
Kim et al. [12]	6144	32	N/A	No
Lee et al. [13]	335.8	50	$-26$	No
Lee et al. [21]	791	120	$-27$	No
Liu et al. [14]	121.6	122	$-38$	No
Liu et al. [27]	190	50	$-26$	No
Kiourti et al. [19]	1063.1	27	$-30$	No
Permana et al. [43]	254	10	$-36.5$	No
Proposed	448	103	$-32$	Yes

Features of other implantable antennas reported in the literature are shown in Table 3. It can be assessed that the antenna presented in this paper achieved the required performance in terms of bandwidth, miniaturization, and gain. Results of received power in this study were in agreement with simulated communication links reported in previous designs of compact implantable antennas. Received power of the antenna presented by Kiourti et al. [20] was  $-56.2$  dBm at a distance of 20 cm from the head, while the antenna presented in this study achieved  $-45.7$  dBm. In addition, obtained received power showed the influence of miniaturization on the transmission channel. Kim et al. [12] evaluated the communication link between a considerably large antenna ( $40\text{ mm} \times 32\text{ mm} \times 8\text{ mm}$ ) implanted into the human chest and an external half-wavelength dipole. When the half-wavelength dipole was located at 30 cm from the phantom-air or skin-air interface, maximum available power was  $-30$  dBm. In the design proposed in our work ( $16 \times 14 \times 2\text{ mm}$ ), available powers ranged from  $-50$  dBm to  $-56$  dBm for the same phantom-air or skin-air to half-wavelength dipole distance. This variation between prototypes was primarily due to the drastic decrease (95.6%) of antenna size.

Computational and experimental approaches were employed in the design and characterization of the miniaturized antenna for an IMD. Strengths of the proposed design to resolve shortcomings of current state-of-the-art in implantable antennas include a balanced performance between a miniaturized design with general volume of  $14 \times 16 \times 2\text{ mm}^3$ , integration of electronic circuits of the IMD with volume up to  $10 \times 10 \times 0.5\text{ mm}^3$ , and an enlarged bandwidth up to 103 MHz in order to consider dielectric properties and geometry disparity of the antenna implanted within various body locations. Satisfactory agreement was found between simulations and measurements of the fabricated antenna implanted into a liquid with dielectric properties of muscle tissue cuboid phantom. Maximum antenna input power was evaluated considering SAR restrictions for 1-g averaged SAR and 10-g averaged SAR for the three body antenna locations. The transmission channel between the proposed antenna and a half-wavelength dipole showed applicability of the antenna up to distances of 1 m while the receptor was capable of operating with a power of  $-60$  to  $-70$  dBm depending on where the antenna was implanted.

This study focused on the simulated performance of the proposed antenna at three body locations and in a muscle tissue cuboid phantom at depths of 15 mm from the phantom-air and skin-air interfaces. Reflection coefficient, transmission channel and radiation pattern were measured for validation purposes in the muscle tissue cuboid phantom. Further evaluation of the antenna implanted at different body locations and variable depths, and acquisition of communication link measurements at other distances are warranted. In this study, the impact of adjacent electronic circuitry on antenna performance was evaluated considering a metallic box as a first approach. Future studies for specific applications should investigate the impact of specific electronic components on the antenna performance. This study considered the antenna implanted in the adult male, further studies will evaluate the implementation of the antenna in an adult female.

## 5. CONCLUSIONS

Design of a compact implantable broadband PIFA for wireless biotelemetry applications is presented in this paper. The antenna was designed to operate in the MedRadio 401–406 MHz frequency band. Modeling analysis was based on electromagnetic calculations using the FDTD method; LTCC multilayer technology was utilized. The proposed antenna, modeled inside fluid that mimics muscle tissue, was simulated when being implanted into the arm, head, and chest of a high-resolution whole-body anatomical model of an adult human male. SAR analysis and impedance mismatch of the antenna inside the human body was considered, and desirable bandwidth enhancement and initial tuning were taken into account. Possible detuning due to the influence of an embedded electronic circuit in the prototype was also assessed. The antenna was manufactured and measurements of the reflection coefficient, transmission level and radiation pattern were made. Simulated and measured results showed satisfactory agreement.

## ACKNOWLEDGMENT

This work was supported in part by the Spanish Secretary of State for Research, Development and Innovation, under project TEC2013-40430-R, and the National Science Foundation (USA), under grant CBET 1337438.

## REFERENCES

1. Chow, E., M. Morris, and P. Irazoqui, "Implantable RF medical devices: The benefits of high-speed communication and much greater communication distances in biomedical applications," *IEEE Microw. Mag.*, Vol. 14, No. 4, 64–73, Jun. 2013.
2. Kiourti, A., K. A. Psathas, and K. S. Nikita, "Implantable and ingestible medical devices with wireless telemetry functionalities: A review of current status and challenges: Implantable/Ingestible medical devices," *Bioelectromagnetics*, Vol. 35, No. 1, 1–15, Jan. 2014.
3. Psathas, K., A. P. Keliris, A. Kiourti, K. S. Nikita, et al., "Operation of ingestible antennas along the gastrointestinal tract: Detuning and performance," *2013 IEEE 13th International Conference on Bioinformatics and Bioengineering (BIBE)*, 1–4, 2013.
4. Weiss, M. D., J. L. Smith, and J. Bach, "RF coupling in a 433-MHz biotelemetry system for an artificial hip," *IEEE Antennas Wirel. Propag. Lett.*, Vol. 8, 916–919, 2009.
5. Crescini, D., E. Sardini, and M. Serpelloni, "Design and test of an autonomous sensor for force measurements in human knee implants," *Sens. Actuators Phys.*, Vol. 166, No. 1, 1–8, Mar. 2011.
6. Kawoos, U., X. Meng, M.-R. Tofighi, and A. Rosen, "Too much pressure: Wireless intracranial pressure monitoring and its application in traumatic brain injuries," *IEEE Microw. Mag.*, Vol. 16, No. 2, 39–53, Mar. 2015.
7. Chow, E. Y., A. L. Chlebowski, S. Chakraborty, W. J. Chappell, and P. P. Irazoqui, "Fully wireless implantable cardiovascular pressure monitor integrated with a medical stent," *IEEE Trans. Biomed. Eng.*, Vol. 57, No. 6, 1487–1496, Jun. 2010.
8. Marnat, L., M. H. Ouda, M. Arsalan, K. Salama, and A. Shamim, "On-chip implantable antennas for wireless power and data transfer in a Glaucoma-monitoring SoC," *IEEE Antennas Wirel. Propag. Lett.*, Vol. 11, 1671–1674, 2012.
9. Karacolak, T., A. Z. Hood, and E. Topsakal, "Design of a dual-band implantable antenna and development of skin mimicking gels for continuous Glucose monitoring," *IEEE Trans. Microw. Theory Tech.*, Vol. 56, No. 4, 1001–1008, Apr. 2008.
10. Soontornpipit, P., C. M. Furse, and Y. C. Chung, "Design of implantable microstrip antenna for communication with medical implants," *IEEE Trans. Microw. Theory Tech.*, Vol. 52, No. 8, 1944–1951, Aug. 2004.
11. Kim, J. and Y. Rahmat-Samii, "Planar inverted-F antennas on implantable medical devices: Meandered type versus spiral type," *Microw. Opt. Technol. Lett.*, Vol. 48, No. 3, 567–572, Mar. 2006.
12. Kim, J. and Y. Rahmat-Samii, "Implanted antennas inside a human body: Simulations, designs, and characterizations," *IEEE Trans. Microw. Theory Tech.*, Vol. 52, No. 8, 1934–1943, Aug. 2004.
13. Lee, C.-M., T.-C. Yo, and C.-H. Luo, "Compact broadband stacked implantable antenna for biotelemetry with medical devices," *2006 WAMICON'06 IEEE Annual Wireless and Microwave Technology Conference*, 1–4, IEEE, 2006.
14. Liu, W.-C., S.-H. Chen, and C.-M. Wu, "Bandwidth enhancement and size reduction of an implantable PIFA antenna for biotelemetry devices," *Microw. Opt. Technol. Lett.*, Vol. 51, No. 3, 755–757, Mar. 2009.
15. Abadia, J., F. Merli, J.-F. Zurcher, J. R. Mosig, and A. K. Skrivervik, "3D-spiral small antenna design and realization for biomedical telemetry in the MICS band," *Radioengineering*, Vol. 18, No. 4, 359–367, 2009.
16. Bakogianni, S. and S. Koulouridis, "Design of a novel compact printed folded dipole antenna for biomedical applications," *2014 8th European Conference on Antennas and Propagation (EuCAP)*, 3178–3182, IEEE, 2014.
17. Yilmaz, T., T. Karacolak, and E. Topsakal, "Characterization and testing of a skin mimicking material for implantable antennas operating at ISM band (2.4 GHz–2.48 GHz)," *IEEE Antennas Wirel. Propag. Lett.*, Vol. 7, 418–420, 2008.
18. Gosalia, K., G. Lazzi, and M. Humayun, "Investigation of a microwave data telemetry link for a retinal prosthesis," *IEEE Trans. Microw. Theory Tech.*, Vol. 52, No. 8, 1925–1933, Aug. 2004.

19. Kiourti, A., K. A. Psathas, J. R. Costa, C. A. Fernandes, and K. S. Nikita, "Dual-band implantable antennas for medical telemetry: A fast design methodology and validation for intra-cranial pressure monitoring," *Progress In Electromagnetics Research*, Vol. 141, 161–183, 2013.
20. Kiourti, A., M. Christopoulou, and K. S. Nikita, "Performance of a novel miniature antenna implanted in the human head for wireless biotelemetry," *2011 IEEE International Symposium on Antennas and Propagation (APSURSI)*, 392–395, IEEE, 2011.
21. Lee, C.-M., T.-C. Yo, F.-J. Huang, and C.-H. Luo, "Bandwidth enhancement of planar inverted-F antenna for implantable biotelemetry," *Microw. Opt. Technol. Lett.*, Vol. 51, No. 3, 749–752, Mar. 2009.
22. Chen, Z. N., G. C. Liu, and T. S. P. See, "Transmission of RF signals between MICS loop antennas in free space and implanted in the human head," *IEEE Trans. Antennas Propag.*, Jun. 2009, Vol. 57, No. 6, 1850–1854.
23. Anacleto, P., P. M. Mendes, E. Gultepe, and D. H. Gracias, "3D small antenna for energy harvesting applications on implantable micro-devices," *2012 Loughborough Antennas and Propagation Conference (LAPC)*, 1–4, IEEE, 2012.
24. Vidal, N., S. Curto, J. M. Lopez-Villegas, J. Sieiro, and F. M. Ramos, "Detuning study of implantable antennas inside the human body," *Progress In Electromagnetics Research*, Vol. 124, 265–283, 2012.
25. Vidal, N., J. M. Lopez-Villegas, S. Curto, J. Colomer, S. Ahyoune, A. Garcia, et al., "Design of an implantable broadband antenna for medical telemetry applications," *2013 7th European Conference on Antennas and Propagation (EuCAP)*, 1133–1136, IEEE, 2013.
26. Furse, C. M., "Biomedical telemetry: Today's opportunities and challenges," *2009 iWAT 2009 IEEE International Workshop on Antenna Technology*, 1–4, IEEE, 2009.
27. Liu, W.-C., F.-M. Yeh, and M. Ghavami, "Miniaturized implantable broadband antenna for biotelemetry communication," *Microw. Opt. Technol. Lett.*, Vol. 50, No. 9, 2407–2409, 2008.
28. Guo, Y.-X. and H. S. Tan, "New compact six-band internal antenna," *IEEE Antennas Wirel. Propag. Lett.*, Vol. 3, No. 1, 295–297, Dec. 2004.
29. Karkkainen, M. K., "Meandered multiband PIFA with coplanar parasitic patches," *IEEE Microw. Wirel. Compon. Lett.*, Vol. 15, No. 10, 630–632, Oct. 2005.
30. Gandara, T. and C. Peixeiro, "Compact triple-band double U-slotted planar inverted-F antenna," *IEEE Int. Symp. Pers. Indoor Mob. Radio Commun.*, 417–421, 2004.
31. Lee, K.-J., T.-K. Lee, and J. W. Lee, "Bandwidth enhanced planar inverted-F antenna with modified ground structure," *2007 APMC 2007 Asia-Pacific Microwave Conference*, IEEE, 1–4, 2007.
32. Feick, R., H. Carrasco, M. Olmos, and H. D. Hristov, "PIFA input bandwidth enhancement by changing feed plate silhouette," *Electron Lett.*, Vol. 40, No. 15, 921–922, 2004.
33. "Medical Implant Communications Service (MICS) federal register," *Rules Regul.*, Vol. 124, No. 240, 69926–69934, 1999.
34. Luo, J. and R. E. Eitel, "A biocompatible low temperature co-fired ceramic substrate for biosensors," *Int. J. Appl. Ceram. Technol.*, Vol. 11, No. 3, 436–442, May 2014.
35. Baras, T. and A. F. Jacob, "Manufacturing reliability of LTCC millimeter-wave passive components," *IEEE Trans. Microw. Theory Tech.*, Vol. 56, No. 11, 2574–2581, Nov. 2008.
36. Golonka, L., P. Bemnowicz, D. Jurkow, K. Malecha, H. Roguszczyk, and R. Tadaszak, "Low temperature co-fired ceramics (LTCC) microsystems," *Opt. Appl.*, Vol. 41, No. 2, 383–388, 2011.
37. Gabriel, S., R. W. Lau, and C. Gabriel, "The dielectric properties of biological tissues: III. Parametric models for the dielectric spectrum of tissues," *Phys. Med. Biol.*, Vol. 41, No. 11, 2271, 1996.
38. Smetana, W., B. Balluch, G. Stangl, E. Gaubitzer, M. Edetsberger, and G. Köhler, "A multi-sensor biological monitoring module built up in LTCC-technology," *Microelectron. Eng.*, Vol. 84, Nos. 5–8, 1240–1243, May 2007.

39. Yee, K., "Numerical solution of initial value problems of maxwells equations," *IEEE Trans. Antennas Propag.*, Vol. 14, No. 3, 302–307, May 1966.
40. Christ, A., W. Kainz, E. G. Hahn, K. Honegger, M. Zefferer, E. Neufeld, et al., "The virtual family — Development of surface-based anatomical models of two adults and two children for dosimetric simulations," *Phys. Med. Biol.*, Vol. 55, No. 2, N23–38, Jan. 21, 2010.
41. Federal Communications Comission, "Evaluating compliance with FCC guidelines for human exposure to radiofrequency electromagnetic fields," Washington, DC, 2001.
42. Warty, R., M.-R. Tofighi, U. Kawoos, and A. Rosen, "Characterization of implantable antennas for intracranial pressure monitoring: Reflection by and transmission through a scalp phantom," *IEEE Trans. Microw. Theory Tech.*, Vol. 56, No. 10, 2366–2376, Oct. 2008.
43. Permana, H., Q. Fang, and W. S. Rowe, "Hermetic implantable antenna inside vitreous humor simulating fluid," *Progress In Electromagnetics Research*, Vol. 133, 571–590, 2013.
44. Skrivervik, A., J.-F. Zurcher, O. Staub, and J. Mosig, "PCS antenna design: The challenge of miniaturization," *IEEE Antennas Propag. Mag.*, Vol. 43, No. 4, 12–27, 2001.
45. Skrivervik, A. and F. Merli, "Design strategies for implantable antennas," *Proc. Loughborough Antennas & Propagation Conference*, Loughborough, UK, 2011.